Journal of Crystal Growth 78 (1986) 135–143
North-Holland, Amsterdam

FERROELECTRIC DOMAIN STRUCTURES IN $LiNbO_3$ SINGLE-CRYSTAL FIBERS

Y.S. LUH and R.S. FEIGELSON

Department of Materials Science and Engineering, Stanford University, Stanford, California 94305-4045, USA

and

M.M. FEJER and R.L. BYER

Department of Applied Physics, Stanford University, Stanford, California 94305-4045, USA

Received 21 April 1986; manuscript received in final form 20 May 1986

The ferroelectric domain structures of small diameter $LiNbO_3$ single crystal fibers were found to be different from those usually observed in large $LiNbO_3$ crystals. *c*-Axis grown fibers with diameters up to 800 μm were found to be virtually single domain with +c end facing the melt during growth. Fibers grown along the *a*-axis had a bi-domain configuration with the domain boundary along the *a*-axis and parallel to the *c*-face. A model is proposed, based on the thermoelectric potential generated by axial and radial temperature gradients, to explain the domain structures observed in these fibers.

1. Introduction

$LiNbO_3$ is a well known ferroelectric material which in single crystal form has found use in a variety of important applications such as nonlinear optical devices, guided wave devices and surface acoustic wave devices. As-grown single crystals usually have a multi-domain structure. Before $LiNbO_3$ can be used in devices, it is necessary to prepare single-domain crystals. Several previous studies [1–7] have been concerned with domain structure morphology and techniques for producing single domain crystals. However, little has been published on the mechanisms which might be responsible for the domain structures observed in this material. In particular, variation of domain structure with crystal size when the diameter is on the order of the domain size is not considered elsewhere.

$LiNbO_3$ crystals are usually grown by the Czochralski method [8]. The domain structures of as-grown crystals were first studied by Nassau et al. [1,3] using a chemical etching method. Multi-domain structures were also reported later by other authors [5–7]. Niizeki et al. [5] found, with the same etching technique, that domain structures could be revealed on opposite *y*-faces as well as on *c*-faces. Since applications for $LiNbO_3$ required single domain crystals, poling processes were developed [1] for rearranging the domain structure. Poling was done either during growth or following growth by heat treatment of the crystal near its melting temperature [2,4]. In both cases an electric field, as small as 0.4 V/cm, applied along the *c*-axis was enough to yield a poled, single domain crystal. Nassau et al. [4] also found that by doping the melt with 0.25 to 1 at% Mo, as grown crystals were sometimes single domain. However, these studies were empirical and explanations were not given for the mechanisms responsible for the morphology observed.

Tasson et al. [9] used the piezoelectric method to study the possible mechanisms responsible for poling of $LiNbO_3$ crystals at temperatures close to the Curie point ($T_C \approx 1210°C$). They concluded that in addition to an applied electric field, concentration and temperature gradients could also influence the domain structure. They attributed both effects to the strain field generated in the crystal. Räuber [8] suggested that the origin of the

0022-0248/86/$03.50

temperature gradient effect may be of thermoelectric nature. Recently, Ming et al. [10] reported on the Czochralski growth of yttrium doped $LiNbO_3$ single crystals with periodic domain structures. These crystals were grown with the rotational axis purposely offset with respect to the symmetry axis of temperature field. They correlated the periodic domains with rotational striations and with striations induced by furnace power fluctuations, and concluded that the domain structures depended on the solute concentration gradient. Feisst and Koidl [11] reported modulated-current-induced, periodic ferroelectric domain structure in Czochralski grown Cr doped $LiNbO_3$ crystals which were studied for applications to nonlinear optical frequency mixing.

Small diameter $LiNbO_3$ crystals (100–800 μm) have been grown by the laser heated pedestal growth method [12,13] for fiber device applications. These single crystal fibers of $LiNbO_3$ exhibited domain structures different from those found previously in Czochralski grown $LiNbO_3$ crystals. This paper reports on the reason for these differences.

2. Experimental

The laser heated pedestal growth (LHPG) method, a variant of the float zone process, is a method for growing small diameter crystals of a wide variety of materials [13]. It is particularly well suited to the growth of oxide materials. Fig. 1 is a schematic illustration of the basic features of LHPG method. A schematic diagram and photograph of the two-beam system can be found in ref. [13]. An improved laser optical system using a paraboloid mirror to produce uniform annular heating was reported by Fejer et al. [14]. Preliminary results on the single crystal fiber growth of $LiNbO_3$ have been reported [12–14].

Using the LHPG method $LiNbO_3$ crystal fibers have been grown both along the c-axis and the a-axis. Typical source rod diameters were 500 μm to 2 mm. With a diameter reduction ratio from source rod to fiber of 2.5 to 1, fibers with diameters ranging from 100 to 800 μm have been grown routinely. Typical growth rates varied from 1 to 3

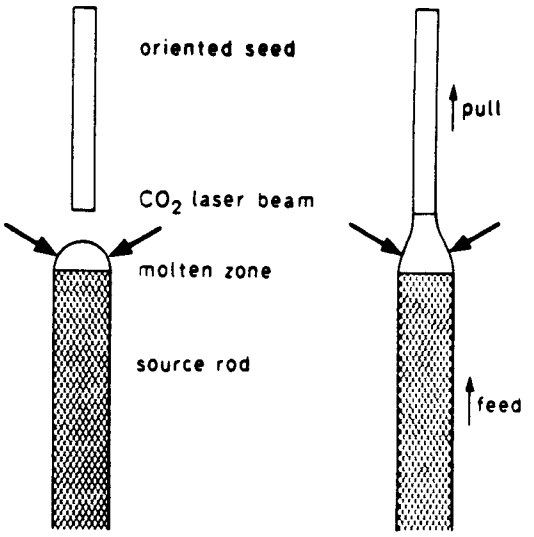

Fig. 1. Schematic diagram of the laser heated pedestal growth method.

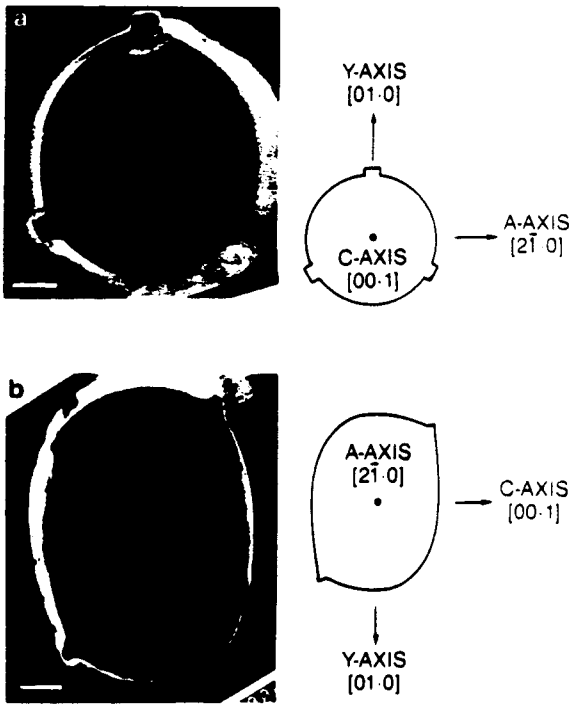

Fig. 2. (a) Cross-section of the cleaved end of a c-axis grown fiber with sketch showing major crystallographic directions; (b) end view of an a-axis grown fiber rapidly separated from the melt with sketch showing the cross-section and major crystallographic directions. Markers represent 100 μm.

mm/min. However, higher growth rates have been used and the upper limit has not been fully explored. Larger diameter crystals were found to crack during growth. It is expected that reducing the temperature gradient above the growth interface might prevent this problem. On the other hand the diameter uniformity was difficult to control in fibers with a diameter of less than 100μm. Single crystal fibers were grown from the congruently melting composition without added dopants.

Fig. 2a shows a cross-section of a fiber grown along the *c*-axis. The characteristic 3-fold symmetry seen in bulk crystals is clearly evident. Three growth ridges separated by 120°C are seen in fig. 2a. The ridges are similar to those seen in larger crystals grown by the Czochralski method, though their shape and relative size are different. Fig. 2a also shows sketch of the major crystallographic orientations. A cross-sectional view and sketch of the major crystallographic orientations in an *a*-axis grown fiber are shown in fig. 2b. The mirror plane of the point group contains the *c*-axis and the *y*-axis and is perpendicular to the *a*-axis. Crystallographic orientations in both *c*-axis and *a*-axis grown crystals were identified by Laue X-ray diffraction analysis and by the optical observation of the isogyre patterns under crossed polarizers.

The etching technique developed by Nassau et al. [1,3] was adapted to reveal the ferroelectric domain structures of the fibers grown by the LHPG method. Fibers were first polished on both sides of the *c*- or *y*-faces, then etched in 1HF + 2HNO_3 solution at 100°C for 5–10 min. The polished face normal was estimated to be off the *c*-axis or *y*-axis by no more than 5°. After etching, the domain structures were observed using an optical microscope and SEM.

3. Results

Fig. 3 shows the typical domain structure found on the *c*-face of a *c*-axis crystal grown by the Czochralski method. The diameter of this crystal is about 1 cm. The crystal contains a domain structure consisting of concentric rings with the number and size of the domains varying. This

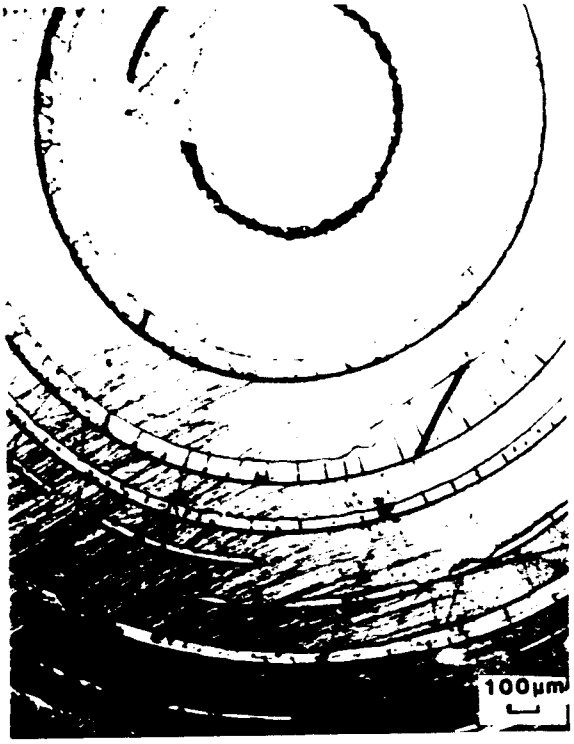

Fig. 3. Ferroelectric domain structures on the *c*-face of a *c*-axis crystal grown by the Czochralski method showing rings of opposite domains.

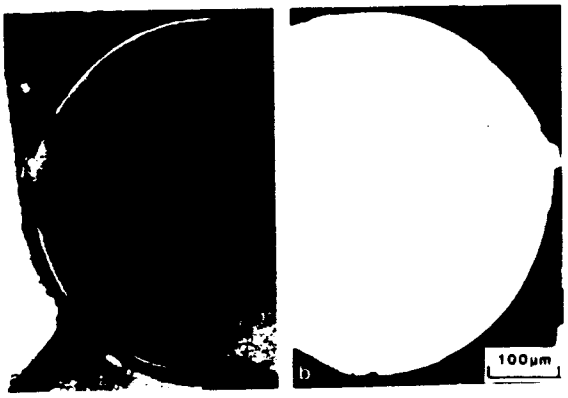

Fig. 4. Domain structures in a 400 μm *c*-axis grown fiber: (a) negative end of the domain with only small anti-parallel domains at the edge; (b) domain structures on the opposite end of the same sample showing mainly a single positive domain. One to one correspondence of the domain structures is obvious.

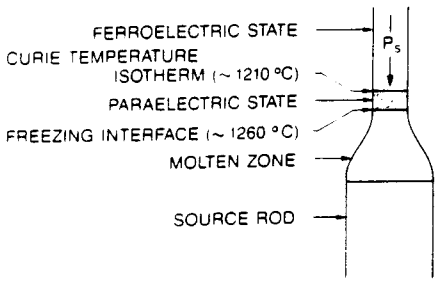

Fig. 5. Schematic diagram showing the domain polarity of a *c*-axis fiber during growth.

result is the same as reported by other authors [1,3,5].

The $LiNbO_3$ fibers grown along the *c*-axis were virtually single domain crystals when the diameter

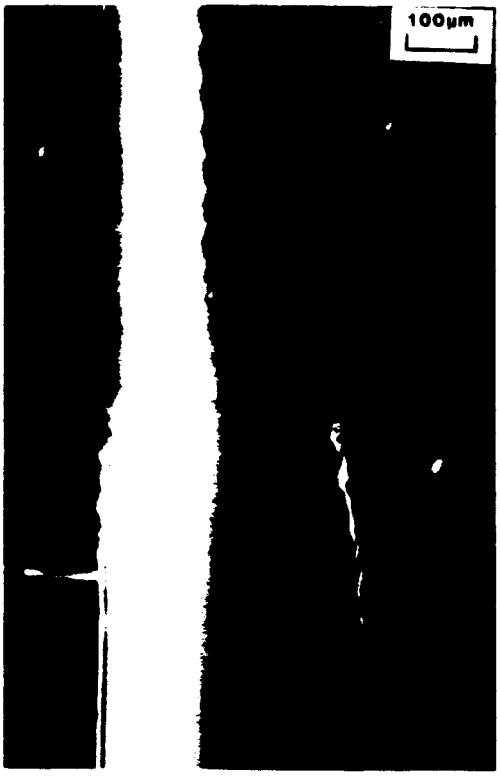

Fig. 6. Rotation of the three growth ridges by 60° can be seen at the seed–fiber interface of this *c*-axis grown fiber. This behavior is only seen when the − *c*-axis of the seed faces the melt.

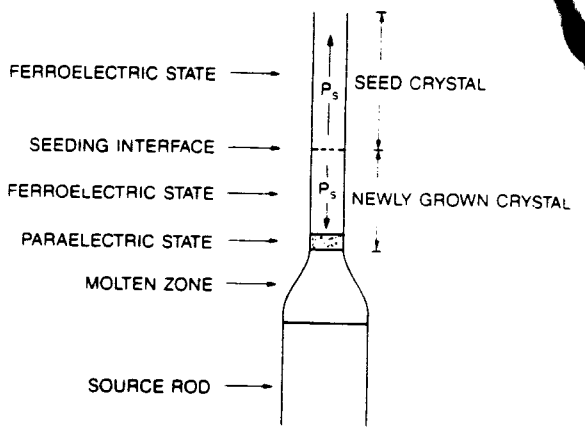

Fig. 7. Schematic diagram summarizing the domain structure of the *c*-axis fiber grown with the conditions shown in fig. 6.

was less than 800 μm. Fig. 4 shows the domain structure on opposite *c*-faces of a 1 cm long *c*-axis grown fiber with a diameter of 400 μm. Fig. 4a is the negative end. Only a very small area of positive domains can be observed at the outer surface of the fiber. Fig. 4b shows the domain structure on the opposite face of the same sample. A one-to-one correspondence between the two domain structures can be readily seen and suggests that the domain structure is preserved throughout the length of the fiber. The positive ends of the ferroelectric domains point toward the melt during growth as illustrated in fig. 5. The orientational

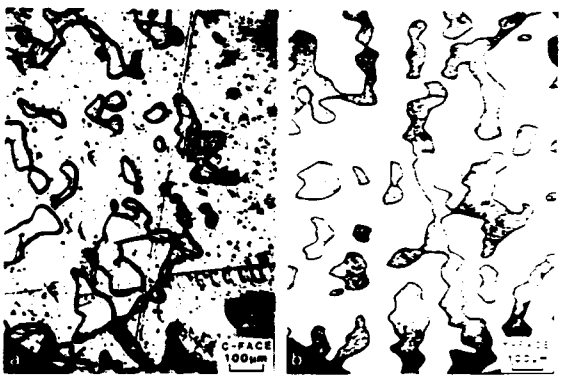

Fig. 8. Domain structure in the *a*-axis crystal grown by the Czochralski method: (a) *c*-face; (b) *y*-face. They both show that the crystal is a multi-domain crystal.

relation between the domain polarity and the temperature gradient is consistent with Tasson et al.'s results [9].

Fibers also were grown with the seed orientation reversed, such that the negative c end of the seed was facing the melt to start the growth. Two interesting results were observed in the reversed seeding growth. First, as shown in fig. 6, a rotation of the growth ridges by 60° was seen immediately when the growth started. This can be understood by the 3-fold roto-inversion symmetry of the crystal in its paraelectric state, in which, after reversing the seed orientation, another set of faceted planes are activated and 3 growth ridges are formed which are rotated 60° in relation to the ridges existing in the seed. Second, while the crystal stayed virtually single domain, the orientation of the spontaneous polarization was reversed in the new growth with the positive end of the domain point toward the melt once again while the seed crystal kept its original domain orientation. This result is schematically shown in fig. 7.

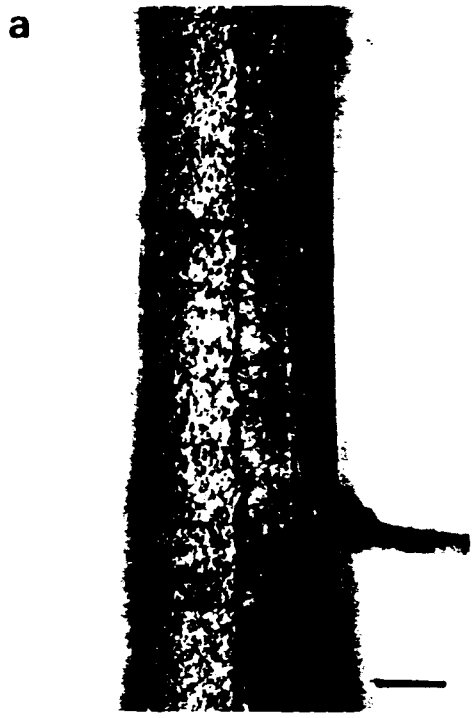

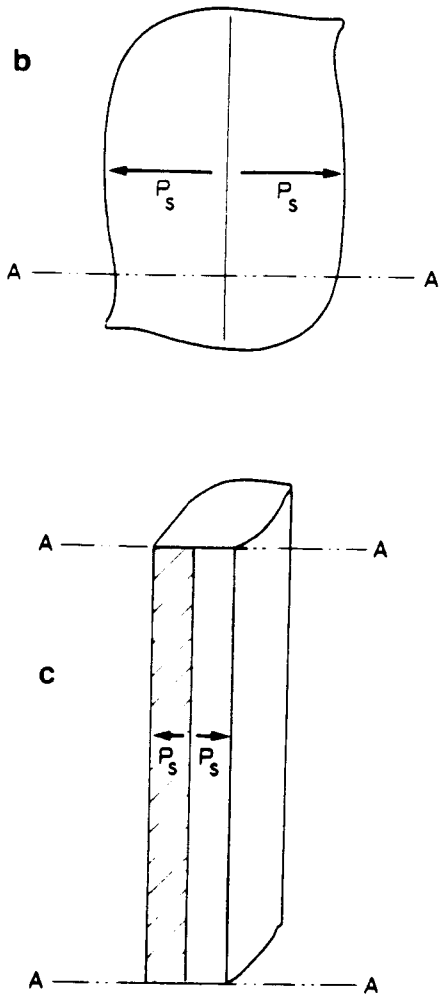

Fig. 9. Domain structures in the a-axis grown fiber: (a) the domain structures seen on y-face; (b), (c) sketches summarizing the domain structures in the a-axis grown fiber. The location of the plane exposed in (c) is indicated by the dashed line in (b). Marker in (a) represents 100 μm.

Regardless of the seed polarity, some potential of fixed sign poles the fiber.

From the point symmetry of $LiNbO_3$ in the ferroelectric state (3m), both the c-axis and the y-axis are polar directions [15]. The opposite faces along the c-axis of y-axis are expected to be different in terms of physical or chemical properties. Fig. 8 shows the domain structures on the c-face and y-face of a typical a-axis crystal grown in our laboratory using the Czochralski method.

The crystals show a random multi-domain structure, with the domain size on the order of a hundred micrometers. These results are consistent with those reported by Niizeki et al. [5] and Ohnish and Lizuka [7].

Unlike the random domain patterns found in large a-axis crystals grown by the Czochralski method, a-axis grown fibers, with cross sections up to 900 μm $\times$ 600 μm, have bi-domain structures with the domain boundary parallel to the c-face. Fig. 9a is a photograph of the domain structures seen on the y-face of an a-axis grown $LiNbO_3$ single crystal fiber. As illustrated schematically in fig. 9b and fig. 9c, the two domains in the a-axis grown fibers are separated by a 180° domain wall with the positive end at the surface as identified by etching the c-faces.

4. Discussion

The equilibrium domain configuration of a ferroelectric is obtained by minimizing the total free energy of the crystal given by

$$G = G_0 + E_e + E_w + E_s + E_t + \ldots, \quad (1)$$

where G = total free energy of the system, E_e = depolarization energy, E_w = domain wall energy, E_s = surface energy, and E_t = strain energy. Some of these terms, such as E_e, favor multi-domain structures, while others, such as E_w, favor a single domain. In the simplest case, when E_s and E_t are neglected, the crystal breaks up into a number of domains such that the reduction of the depolarization energy is balanced by an increase in the domain wall energy [16]. These simplified energy considerations can explain the concentric rings of opposite domains in c-axis crystals and the random domains observed in a-axis crystals.

As the diameter of a c-axis crystal approaches the equilibrium domain size found in bulk crystals, a single domain structure minimizes the free energy. This is consistent with our observations. However, the preferred domain polarity in the c-axis grown fiber cannot be explained by the depolarization and domain wall energies alone. In addition, the back-to-back dipole moments at the seed–crystal interface of a reversed seeding c-axis fiber growth is a maximum energy state. Similarly, the simplified energy considerations cannot explain the domain structures seen in a-axis grown fibers. The bi-domain structure with back-to-back dipole moments is a higher energy configuration than a single domain structure. Therefore it is reasonable to assume that a self-generated bias is responsible for the poling effect found in the fiber growth.

The temperature gradients present during fiber growth are significantly larger than those typically found during Czochralski growth. Since the pyroelectric, piezoelectric and thermoelectric effects all can lead to the formation of a potential difference in a temperature gradient, it is logical to consider the possibility of a self-generated electric poling field being due to one or more of these effects. From the point symmetry of $LiNbO_3$ in the paraelectric state, i.e. $\bar{3}$m, the coefficients of all pyroelectric and piezoelectric tensors are equal to zero. In the ferroelectric state a reversal of the crystal orientation implies a sign change of the coefficients in the pyroelectric tensor (first rank) and piezoelectric tensor (third rank). It appears that neither pyroelectric nor piezoelectric effects can explain the reversed seeding experiment.

On the other hand, the thermoelectric field, E, generated in the material due to a temperature gradient, ∇T, seems consistent with our experimental observations. This electric field can be expressed as

$$E = Q \nabla T, \quad (2)$$

where Q is the thermoelectric power tensor, which is of second rank and has non-vanishing coefficients both in the paraelectric and ferroelectric states. Jorgensen and Bartlett [17] have reported the thermoelectric power of $LiNbO_3$ in a $50CO/50CO_2$ atmosphere. They found that the thermoelectric power of $LiNbO_3$ is 0.55 mV/°C at 1150°C and increases slightly as the temperature decreased. We measured the thermoelectric power of $LiNbO_3$ in air, the same atmosphere in which we grew fibers, by placing the crystal in a temperature gradient of about 10°C/cm and then measuring the potential and temperature difference developed between the thermocouples leads. We found that Q_{33} of $LiNbO_3$ is on the

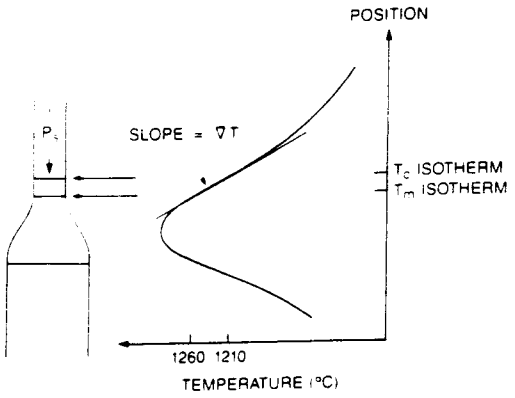

Fig. 10. Qualitative temperature profile in the fiber and estimate of the temperature gradient near the growth interface. T_c is the Curie temperature. T_m is the melting temperature, source rod diameter ≈ 1 mm, fiber diameter ≈ 400 μm, temperature gradient at the growth interface ≈ 1000 °C/cm.

order of 0.4 mV/°C at a temperature close to the melting point.

The temperature gradient along the growth axis near the growth interface is estimated to be greater than 1000 °C/cm as shown schematically in fig. 10. This is one order of magnitude greater than that used in the poling mechanism study by Tasson et al. [9]. The product of this estimated temperature gradient and Q_{33} results in an electric field on the order of 1 V/cm. This field is greater than the poling field used by Nassau et al. [4] to pole crystals during or after growth. Thus it is reasonable to assume that the field generated by the thermoelectric effect is responsible for the poling effect observed in the *c*-axis grown fibers. We believe that the thermoelectric effect plays the same role in Czochralski growth. However, in the latter case, due to much smaller temperature gradients and much larger crystal diameter, the depolarization and domain wall energies play more important roles in determining the equilibrium domain configurations.

To account for the domain structures observed in the *a*-axis grown fibers, we need to analyze the

Fig. 11. Analysis of the temperature gradient and prediction of the domain structure in the *a*-axis grown fiber: (a) sketch of growth interface seen during growth; (b) grown-in interface seen on *y*-face, also shows the bi-domain structures of the *a*-axis fiber; (c) actual temperature gradient at the growth interface; (d) projection of the temperature gradient on the *c*-axis near the growth interface; (e) prediction of domain structures in the *a*-axis fiber based on the thermoelectric model. Marker in (b) represents 100 μm.

radial temperature gradient at the Curie isotherm. Since the axial temperature gradient near the growth interface is so large and the Curie point is only about 50°C below the melting temperature, it is reasonable to assume that the Curie isotherm and the growth interface are close together and have the same shape. The growth interface is convex toward the melt. Fig. 11a is a schematic of the growth zone. A photograph of the polished section of a rapidly cooled growth zone, with the curved boundary between the fibers and the melt clearly evident, is shown in fig. 11b. The total temperature gradient and resolved gradient along the *c*-axis near the growth interface are shown in fig. 11c and fig. 11d. From the resolved temperature gradient and the proposed thermoelectric model, we can predict that the domain structures should appear as illustrated in fig. 11e. This structure can clearly be seen in fig. 9a and fig. 11b. From the sketch in fig. 11d it can be seen that the radial temperature gradient (along *c*-axis) is greater at the edge, becomes smaller toward the center, and changes sign when it crosses the domain boundary. The small multi-domain region seen at the domain boundary can be explained by the small field near the center of the fiber, where the radial temperature gradient is near zero.

To further test the thermoelectric model, we modified the domain structures by modifying the growth interface as depicted in fig. 12a. Here the radial temperature gradient is shifted from a symmetric to an asymmetric position with respect to the fiber axis by asymmetrically heating the molten zone. Fig. 13 shows ferroelectric domain structures and the growth interface corresponding to the case in fig. 12a. It can be seen that the polarization boundary shifts to match the configuration of the modified temperature gradient. The thermoelectric model correctly predicts the observed domain structure in both *a*-axis and *c*-axis fibers.

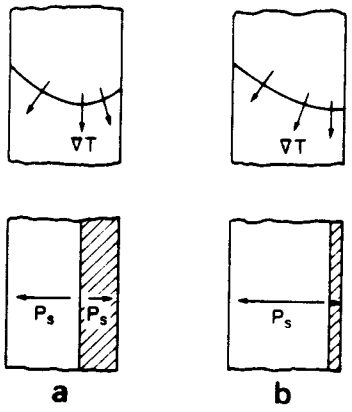

Fig. 12. Predictions of ferroelectric domain structures in *a*-axis fibers based on the thermoelectric model with increasingly asymmetrical heating.

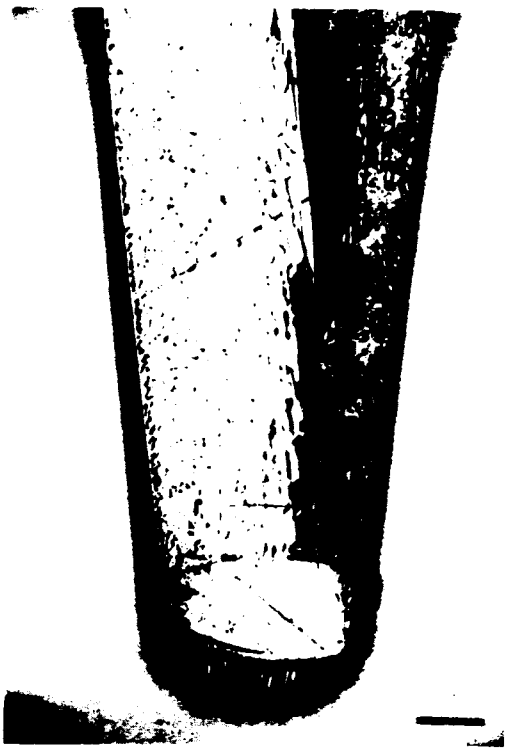

Fig. 13. Domain structures and growth interface shape corresponding to the situation in fig. 12a. Marker represents 100 μm.

5. Conclusions

$LiNbO_3$ single crystal fibers have been grown along both the *c*-axis and the *a*-axis with diameters between 100 and 800 μm. Unlike the multi-ferroelectric-domain structure found in large crystals, fibers grown along the *c*-axis with diam-

eters up to 800 μm were virtually single domain. *a*-Axis grown fibers showed a bi-domain configuration with a domain boundary along the *a*-axis and parallel to the *c*-face. We have confirmed that the direction of spontaneous polarization is the same as the temperature gradient. Our proposed model, based on the thermoelectric effect, explains the self-poling behavior. The understanding of $LiNbO_3$ ferroelectric domain alignment based on the thermoelectric model may lead to techniques for the fabrication of fibers with controlled periodic domain structures that are potentially useful in nonlinear optical interactions.

Acknowledgments

The authors would like to express their appreciation to Dr. R.K. Route, Dr. J.L. Nightingale, Mei Lü, Wayne Kway and M.M. Elwell for helpful discussions and comments. This work was supported by the NSF–MRL program through the Center for Materials Research at Stanford University.

Rereferences

[1] K. Nassau, H.J. Levinstein and G.M. Loiacono, Appl. Phys. Letters 6 (1965) 228.
[2] K. Nassau and H.J. Levinstein, Appl. Phys. Letters 7 (1965) 69.
[3] K. Nassau, H.J. Levinstein and G.M. Loiacono, J. Phys. Chem. Solids 27 (1966) 983.
[4] K. Nassau, H.J. Levinstein and G.M. Loiacono, J. Phys. Chem. Solids 27 (1966) 989.
[5] N. Niizeki, T. Yamada and H. Toyoda, Japan. J. Appl. Phys. 6 (1967) 318.
[6] H.T. Parfitt and D.S. Robertson, Brit. J. Appl. Phys. 18 (1967) 1709.
[7] N. Ohnishi and T. Iizuka, J. Appl. Phys. 46 (1975) 1063.
[8] A. Räuber, in: Current Topics in Materials Science, Vol. 1, Ed. E. Kaldis (North-Holland, Amsterdam 1978).
[9] M. Tasson, H. Legal, J.C. Gay, J.C. Peuzin and F.C. Lissalde, Ferroelectrics 13 (1976) 479.
[10] N.B. Ming, J.F. Hong and D. Feng, I. Mater. Sci. 17 (1982) 1663.
[11] A. Feisst and P. Koidl, Appl. Phys. Letters 47 (1985) 1125.
[12] M.M. Fejer, R.L. Byer, R.S. Feigelson and W.L. Kway, in: Proc. SPIE, Vol. 320, Advances in Infrared Fibers II (1982) p. 50.
[13] R.S. Feigelson, W.L. Kway and R.K. Route, in: Proc. SPIE, Vol. 484, Infrared Optical Materials and Fibers III (1984) p. 133.
[14] M.M. Fejer, J.L. Nightingale, G.A. Magel and R.L. Byer, Rev. Sci. Instr. 55 (1984) 1791.
[15] J.F. Nye, Physical Properties of Crystals (Clarendon, Oxford, 1957).
[16] M.E. Lines and A.M. Glass, Principles and Applications of Ferroelectrics and Related Materials (Clarendon, Oxford, 1977).
[17] P.J. Jorgensen and R.W. Bartlett, J. Chem. Phys. Solids 30 (1969) 2639.